Meccanica (2021) 56:1575–1586
https://doi.org/10.1007/s11012-020-01154-w

RECENT ADVANCES IN COMPUTATIONAL MECHANICS AND INNOVATIVE MATERIALS

Bayesian estimation of single ply anisotropic elastic constants from spherical indentations on multi-laminate polymer-matrix fiber-reinforced composite samples

Andrew R. Castillo · Surya R. Kalidindi

Received: 21 January 2020 / Accepted: 25 March 2020 / Published online: 6 April 2020

Abstract In this paper, the application of a recently formulated two-step Bayesian framework to the estimation of effective anisotropic elastic constants of single plies within a multi-laminate polymer matrix composite is demonstrated, while using previously reported spherical indentation measurements within singular plies. Experimental spherical indentation measurements within the epoxy/fiber plies are inherently noisy due to local variation of the fiber volume fraction underneath the indenter. This paper demonstrates that the usage of a two-step Bayesian framework enables the extraction of reliable point estimates (and associated distributions) for the effective elastic constants from indentation modulus measurements conducted within single plies at different angles to the fiber orientations. The first step of the two-step Bayesian framework establishes the effective elastic indentation modulus of a single ply as a function of its intrinsic elastic stiffness parameters and the angle between the indentation direction and the fiber orientation using a database of suitable finite element simulations. The second step involves the calibration of the indentation measurements from a given set of multi-laminate samples to the reduced-order model established in the first step. The second step is accomplished by sampling the posterior distribution of the single ply elastic parameters via Monte Carlo Markov Chain methods. This new framework is demonstrated in this study for an IM7/977-3 carbon fiber/epoxy multi-laminate sample.

Keywords Polymer-matrix composites · Mechanical properties · Bayesian inference · Monte Carlo · Reduced order models · Spherical indentation

1 Introduction

Laminated polymer matrix composites (PMC), comprised of stacked layers (referred as a laminate or multi-laminate) with each layer consisting of fibers orientated in a single direction (referred as a ply), have offered high tailorability and potential for the optimization of the mechanical properties to various applications across automotive, aerospace and civil infrastructure industries [1–4]. The modeling of the mechanical properties of the multi-laminate composite is generally pursued using homogenization schemes at two scales. At the first level, one takes the fiber and matrix properties and fiber volume fraction as inputs, and estimates the effective anisotropic properties of a singular ply [5, 6]. At the second

In honor of Professor J.N. Reddy for his 75th Birthday.

A. R. Castillo · S. R. Kalidindi (✉)
George W. Woodruff School of Mechanical Engineering, Georgia Institute of Technology, Atlanta, GA 30332, USA
e-mail: surya.kalidindi@me.gatech.edu

level, one takes the laminate properties and geometry (including stacking sequence and thicknesses of the individual plies) as inputs, and estimates the effective anisotropic properties of the PMC [7–12]. Consequently, the effective properties of a single ply play a critical role in the design of the laminated PMCs tailored for a selected application. Direct experimental validation of the two-level composite models has been hampered by the lack of experimental protocols for the reliable estimation of the ply properties in a given multi-laminate sample [9, 13–16]. The current practice relies on making single ply samples for experimental evaluation of their mechanical properties. However, one cannot be confident that the properties measured from these single ply samples would correspond well with the properties of the individual plies in a multi-laminate sample, because there are unavoidable differences in the processing conditions experienced in the production of these different samples.

Indentation techniques have been widely used in prior literature for establishing the local properties in heterogeneous samples, mostly aimed at evaluating the properties of microscale constituents or interfaces [17–20]. Recent advances in indentation instrumentation have tremendously improved the measurement resolution limits, and have now made it possible to measure local properties at submicron length scales. More specifically, recently developed spherical indentation protocols have demonstrated the consistent extraction of crystal-level indentation stress–strain responses from sub-granular load–displacement indentation measurements on polycrystalline metal samples [21–25]. These recent protocols are able to extract reliably the grain-level (i.e., grain lattice orientation dependent) indentation properties such as indentation modulus and indentation yield strength. Even more recently, novel protocols based on Bayesian statistics have been developed for estimating the intrinsic single crystal material properties (e.g., single crystal elastic stiffness parameters such as C_{11}, C_{12}, and C_{44} or the critical resolved shear strength) from the grain orientation-dependent indentation properties measured in different grains in a polycrystalline sample. These protocols fundamentally tackle an inverse problem that calibrates the values of the intrinsic material properties of interest by matching the forward numerical (i.e., finite element method) solutions to the measurements obtained in the indentation experiments performed on a polycrystalline sample [26–28].

The spherical indentation stress–strain protocols have recently been extended to studies in carbon fiber/epoxy laminate composite. In a recent study, the spherical indentation stress–strain protocols were demonstrated for various orientations of single plies within a multi-laminate system [29]. Indentation moduli and indentation yield strengths at different declination angles (i.e., angle between the indentation direction and the fiber direction in a single ply) were reliably extracted from a multi-laminate PMC sample. The measured values of the indentation moduli were shown to decrease dramatically with an increase in declination angle, and were found to be reasonably consistent with forward predictions from finite element simulations. This recent study has demonstrated the potential of the spherical indentation stress–strain protocols for obtaining reliable and repeatable measurements of the local mechanical response of a single ply from a multi-laminate PMC sample. The next logical step in this research is to explore methods to extract the homogenized intrinsic properties of the individual plies from the indentation moduli measured at different declination angles (by indenting the differently oriented plies in a multi-laminate PMC sample). More specifically, the homogenized elastic response of a single ply (each ply is a composite comprising matrix and fibers) can be assumed to exhibit transverse isotropy and is represented by a set of five intrinsic stiffness parameters denoted as C_{11}, C_{12}, C_{13}, C_{33}, and C_{44}; these five parameters are adequate to fully define the ply's fourth-rank elastic stiffness tensor.

As already mentioned, the estimation of the intrinsic materials properties from the indentation properties demands a difficult inverse solution. This is because the most reliable forward models for this problem require the use of a computationally intensive finite element (FE) model of the indentation test. For the present case, the forward model would take the single ply properties as inputs, and predicts the indentation stress–strain responses at different declination angles. Given the high computational cost of the FE models of the indentation tests, inverse solutions need an efficient strategy. In recent work [26], a two-step Bayesian framework was proposed to address this class of problems, and its viability was demonstrated with the extraction of intrinsic crystal-

level properties from indentation measurements in polycrystalline cubic and hcp metal samples. The first step in this protocol establishes a high fidelity, low computational cost, reduced-order model to take place of the computationally intensive FE model of the spherical indentation test. The second step calibrates the single ply properties of interest by using the experimentally measured indentation properties at different declination angles using the reduced-order model established in the first step together with a Monte Carlo Markov Chain (MCMC). One of the salient aspects of the proposed two-step Bayesian framework is that it also provides an estimate of the uncertainty (quantified as variance) in the estimated intrinsic properties. In this work, we will extend and demonstrate the viability of using the two-step Bayesian framework for the estimation of the single ply elastic stiffness parameters from the spherical indentation measurements on a multi-laminate PMC sample. It should be noted that the PMC samples studied here exhibit significantly higher levels of anisotropy and inherent variance in the indentation measurements, when compared to the polycrystalline cubic and hcp metal samples studied earlier.

2 Methods

2.1 Experimental data

The elastic contact between two isotropic homogenous bodies with quadratic surfaces is described by Hertz theory as

$$P = \frac{4}{3} E^* R_{eff}^{\frac{1}{2}} h_e^{\frac{3}{2}} \tag{1}$$

where P is the indenter load,h_e is the elastic indentation displacement, R_{eff} is the effective radius of the indenter-sample system, and E^* is the effective indentation modulus. Although the measured E^* generally reflects the effective indentation modulus of the indenter-sample system, one can account for the elastic deformation in the indenter itself and recover the indentation modulus of the sample alone [30]. In the treatment presented here, it will be assumed that such corrections have been made, i.e., E^* denotes the indentation modulus of the sample. In recent work [29], spherical indentation protocols were used successfully to measure the effective indentation moduli at four different declination angles (denoted by ϕ) for single plies in an IM7/977-3 carbon fiber/epoxy multi-laminate sample. These measurements are summarized in Table 1, and are used in this study for the estimation of the single ply elastic constants. Note that the measurements show that the indentation moduli decrease significantly with an increase in the declination angle, and exhibit high levels of variance in the measurements. The high variance was attributed to the expected large variance in the local fiber volume fractions in the primary zones of the indentations performed [29].

2.2 Finite element models for effective indentation moduli of plies

The simulated domain is treated as homogenous, transversely isotropic solid, whose elastic response in the sample reference frame is fully described by the set of five elastic constants, $\boldsymbol{c} = \{C_{11}, C_{12}, C_{44}, C_{33}, C_{13}\}$ and the specified declination angle, ϕ, between the fiber orientation in the single ply and the indentation direction. The sample size simulated was chosen to be 670 μm × 670 μm × 335 μm, while the indenter radius was chosen to be 500 μm, consistent with the experiments. The simulated sample size was chosen to be much larger than the indentation zone size ($\sim$ 50 μm reported in experiments) [29]. The mesh used is adopted from prior work, and consisted of 12,610 C3D8 continuum 3-D elements [27, 29]. The FE model used in this work has been previously validated for the extraction of effective indentation moduli of various material systems, including cubic metal single crystals [27] and hexagonal metal single crystals [26]. The FE model has also been validated by direct comparisons with the analytical solutions reported by Vlassak and Nix [19]. Most recently, this FE model has been validated through the direct comparison of simulated and experimental values in single plies within PMC multi-laminate samples [29].

2.3 Bayesian framework for the extraction of intrinsic material properties

The Bayesian framework employed here is adopted from prior work [26], and is briefly reviewed next. In this approach, the measured experimental indentation modulus for the ith ply orientation (i.e., declination angle, ϕ) is modeled as

Table 1 Previously reported measured indentation moduli for single plies in an IM7/977-3 carbon fiber/epoxy multi-laminate sample [29]

Ply Orientation (ϕ)	Number of Tests	Mean Indentation Modulus (GPa)	Standard Deviation (GPa)
0	29	43.2	8.7
30	14	29.9	4.0
60	18	16.6	1.7
90	28	12.4	3.0

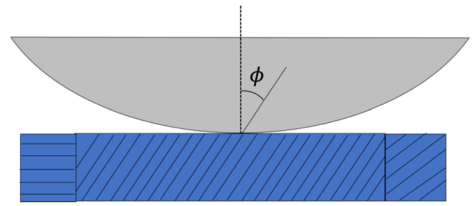

$$E_i^* = E_{sim}^*(\boldsymbol{c}, \phi_i) + \epsilon_i \tag{2}$$

where $E_{sim}^*(\boldsymbol{c}, \phi_i)$ denotes the FE-simulated indentation modulus corresponding to a set of effective elastic constants and a single ply orientation, and $\epsilon_i \sim \mathcal{N}(0, \sigma_i^2)$ denotes a stochastic noise term. It is implicitly assumed here that the FE simulated $E_{sim}^*(\boldsymbol{c}, \phi_i)$ exhibits negligible variance. Let $\{\boldsymbol{E}_{exp}^*, \boldsymbol{\Phi}_{exp}\}$ denote the set of experimental indentation moduli, $\boldsymbol{E}_{exp}^*$, measured at the corresponding ply orientations, $\boldsymbol{\Phi}_{exp}$. The likelihood for n experimental measurements across multiple plies (denoted $\{\boldsymbol{E}_{exp}^*, \boldsymbol{\Phi}_{exp}\}$) is expressed as

$$p\left(\boldsymbol{E}_{exp}^* | \boldsymbol{c}, \boldsymbol{\Phi}_{exp}\right) = \prod_i^n \frac{1}{\sqrt{2\pi}\sigma_i} exp\left\{\frac{-\left(E_i^* - E_{sim}^*(\boldsymbol{c}, \phi_i)\right)^2}{2\sigma_i^2}\right\} \tag{3}$$

where the variance, σ_i^2, is directly measured from experiments in the i-th ply (with a declination angle, ϕ_i). Inference of the effective elastic constants, $\boldsymbol{c}$, for the observed experimental data can be expressed by Bayes rule:

$$p\left(\boldsymbol{c} | \boldsymbol{E}_{exp}^*, \boldsymbol{\Phi}_{exp}\right) \propto p\left(\boldsymbol{E}_{exp}^* | \boldsymbol{c}, \boldsymbol{\Phi}_{exp}\right) p(\boldsymbol{c}) \tag{4}$$

Assuming a uniform prior for $p(\boldsymbol{c})$ along with the likelihood function shown in Eq. (3), Eq. (4) allows for the application of MCMC methods for sampling the posterior distribution on the effective intrinsic material properties [31, 32]. MCMC algorithms seek to generate a sequence, known as a Markov Chain, which converges to a target posterior distribution by accepting/rejecting a large number of proposed transitions across a finite parameter space based on an acceptance probability [26]. Specifically, the Single Component Metropolis–Hastings (SCMH) algorithm is adopted in this work to generate transitions across the multivariate parameter space of effective elastic constants [26, 31]. When implementing SCMH, the acceptance probability of a transition is solely determined by the ratio between candidate and current values evaluated by Eq. (4). In practice, these methods often require tens of thousands of evaluations of the likelihood function to ensure convergence [33]. In this work, 50,000 samples are drawn via SCMH in order to generate a Markov Chain. Due to the probabilistic nature of MCMC, it is desirable to run the algorithm multiple times, randomly selecting initial starting points to ensure that independently sampled Markov Chains converge to similar distributions. The high computational costs associated with the execution of the FE models of indentation make it impractical to use the FE indentation models directly in the computations described above. The only practical approach for addressing this challenge is to first establish a reduced-order model.

Recent work [26] has demonstrated the successful development of a reduced-order model that captures the dependence of indentation modulus on the crystal orientation of the indented grain and an arbitrary set of single crystal elastic constants. The development of this reduced-order model involved the use of an expanded Fourier basis and the calibration of the Fourier coefficients via Bayesian Linear Regression (BLR). The usage of BLR provides a valuable quantification of uncertainty associated with the predictions from the reduced-order model [34]. These

same strategies are adopted in this work to establish a reduced-order model for $E^*_{sim}(\boldsymbol{c}, \phi)$. In order to establish the reduced-order model, a database of finite element simulations covering the relevant input parameter space is necessary. The quantification of uncertainty provided by BLR enables the deployment of sequential strategies to build a simulated database by focusing on areas of high predictive uncertainty. Simulations can be continually performed until sufficient performance of the reduced-order model is achieved, as determined by various error metrics. The implementation of this strategy in previous work has shown a significant reduction in the number of simulations necessary to establish a high fidelity reduced-order model in comparison with traditional regression approaches [26, 27].

The Fourier basis used in the development of a reduced-order model in the previous work were obtained by compounding symmetrized surface spherical harmonics (to represent functions over the orientation space) with Legendre polynomials (to represent functions over the ranges of the values for the single crystal material constants) [26, 27]. The advantage of this representation was the ability to capture the underlying crystal symmetries exhibited by the material system. We note that the local orientation of any material system with respect to a defined sample frame can be represented by a set of Bunge Euler angles $\{\varphi_1, \phi, \varphi_2\}$ [35]. Since any rotation about the sample normal does not affect the measured indentation properties, it can be seen that the indentation properties are independent of φ_1 [19, 35, 36]. Furthermore, the indentation modulus of the transversely isotropic material simulated in this work is also independent of φ_2 (i.e., a rotation of the ply about the fiber axis also does not influence the measured indentation response). As a result of these considerations, the desired reduced-order model [26] can be expressed as

$$E^*_{sim} \approx \hat{E^*}(\boldsymbol{c}, \phi) = \sum_{l=0}^{L} \sum_{\boldsymbol{q}}^{\boldsymbol{Q}} A^{l\boldsymbol{q}} P^l(cos(\phi)) \tilde{P^{\boldsymbol{q}}}(\bar{\boldsymbol{c}}) \tag{5}$$

$$\bar{c_j} = \frac{2c_j - c_j^{min} - c_j^{max}}{c_j^{max} - c_j^{min}} \tag{6}$$

where $P^l(\cos\phi)$ denote Legendre polynomials expanded over the ply orientation space [35], and $\tilde{P^{\boldsymbol{q}}}(\bar{\boldsymbol{c}})$ denote a multivariate Legendre polynomial product basis. In other words, one can express $\tilde{P^{\boldsymbol{q}}}(\bar{\boldsymbol{c}}) = P^{q_1}(\bar{c}_{11}) P^{q_2}(\bar{c}_{12}) P^{q_3}(\bar{c}_{44}) P^{q_4}(\bar{c}_{33}) P^{q_5}(\bar{c}_{13})$, where $\boldsymbol{q} = (q_1, q_2, q_3, q_4, q_5)$ forms a multi-index array, each element of which is a nonnegative integer allowed to vary from 0 to the selected maximum degree, Q, i.e., $q_j \in [0, Q]$. For the proper application of the Legendre Polynomial basis, each of the elastic constants are rescaled over their respective ranges [37] as shown in Eq. (6), where c_j^{max} and c_j^{min} are the maximum and minimum values of the j-th elastic constant. $\boldsymbol{Q}$ and L denote the truncation levels adopted in the formulation of Eq. (5). We note that the degree of the Legendre polynomials expanded about the orientation space are selected to be strictly even to fully reflect the symmetries present in the transversely isotropic material system [35]. The model coefficients, $\boldsymbol{A}$, are established using the aforementioned sequential model building process deployed successfully in previous work [26].

3 Results

3.1 Reduced-order model building

In order to evaluate the likelihood function in Eq. (3), a high fidelity reduced-order model must be established covering a suitable parameter space of the elastic intrinsic material parameters. The first step in this process is the identification of the extent of the input parameter space to be covered by the reduced-order model. To identify this space, simplified estimates of the effective elastic properties of a ply [6] can be computed using the constituent fiber/matrix properties in the following equations:

$$E_3 = E_{f3} V_f + E_m V_m \tag{7}$$

$$E_1 = E_2 = \frac{E_m}{1 - \sqrt{V_f}\left(1 - {E_m}/{E_{f2}}\right)} \tag{8}$$

$$G_{23} = G_{13} = \frac{G_m}{1 - \sqrt{V_f}\left(1 - {G_m}/{G_{f23}}\right)} \tag{9}$$

$$G_{12} = \frac{G_m}{1 - \sqrt{V_f}\left(1 - {G_m}/{G_{f12}}\right)} \tag{10}$$

$$v_{23} = v_{f23} V_f + v_m V_m \tag{11}$$

Table 2 Bounds of each elastic stiffness constant considered in this study. Bounds were computed in accordance to Eqs. (7–11) considering a fiber volume fraction between 20 and 80%

	C_{11} (GPa)	C_{12} (GPa)	C_{44} (GPa)	C_{33} (GPa)	C_{13} (GPa)
Max	30.8	22.1	7.7	239	16.7
Min	5.6	1.3	2.2	65.9	2.2

where E, G, v denote the Young's moduli, shear moduli, and Poisson's ratios, respectively, the fiber direction corresponds to the 3-axis, and the subscripts m and f refer to the matrix and the fiber components, respectively [5]. A range of fiber volume fraction, V_f, between 20 and 80% was used in Eqs. (7–11) in order to delineate the domain of the input parameter space for the desired reduced-order model. For these computations, the constituent fiber and matrix properties were taken from manufacturers' data (Hexcel HexTow IM7, CYCOM 977-3 Epoxy Resin) and reported values in literature [29, 38, 39]. The fiber properties were set as $E_{f3} = 276$ GPa, $E_{f1} = 26$ GPa, $G_{f12} = 7$ GPa, $G_{f23} = 20$ GPa, $v_{f23} = 0.3$, while the matrix properties were set as $E_m = 3.3$ GPa, $G_m = 1.2$ GPa, $v_m = 0.35$. The ply stiffness values computed from Eqs. (7–11) were then converted to the corresponding values of $\boldsymbol{c}$ used in the development of the framework presented in this paper using relations already established in literature [5]. The extents (i.e., ranges) for the values of the components of $\boldsymbol{c}$ covered by the present work are summarized in Table 2. The full range of the ply orientation space, $0 \leq \phi \leq 90$ degrees, was included in this work.

As previously mentioned, a sequential model building process is adopted from prior work [26] in order to efficiently establish a reduced order model within the identified input parameter space. The implementation of this process includes the establishment of an initial reduced-order model using an initial data set, followed by the selection of additional simulations based on predictive uncertainty. An initial data set of 740 simulations was generated from unique sets of inputs, $\{\boldsymbol{c}, \phi\}$, determined by a Max-Pro Latin Hypercube Design within the extents of the parameter space identified in Table 2, while ensuring material stability (i.e., positive eigen values for the stiffness tensor) [40, 41]. The number of simulations for the initial data set was selected to be close to the number of coefficients associated with a reduced-order model established for the single crystal elastic constants in hcp crystals (i.e., truncation level Q = 2, L = 4 resulting in 729 model coefficients) [26]. Inputs to additional simulations were selected from another Max-Pro Latin Hypercube Design of 2200 simulations in accordance with the sequential model building strategy adopted from previous work [26].

Given the high levels of anisotropy in the composite plys studied here compared to the hcp crystals studied in previous work [26], it was anticipated that a higher level of truncation would be necessary for the present work. Using cross-validation error (CVE) approaches [42], the aforementioned model building process identified that a truncation level of Q = 2, L = 6 (CVE = 0.93 GPa) provides significant improvement over the truncation level Q = 2, L = 4 (CVE = 1.57 GPa) for the present work. The necessity of higher model complexity for the present case compared to the previous work [26] involving hexagonal single crystals is quite reasonable due to a notable increase in the anisotropy in the present work. The degree of elastic anisotropy can be quantified by the universal elastic anisotropic index, $\mathbb{A}$, defined as [43]

$$\mathbb{A} = 5\frac{G_v}{G_r} + \frac{K_v}{K_r} - 6 \tag{12}$$

where K and G are the bulk and shear moduli provided by Voigt and Reuss estimates (indicated by subscript v and r, respectively) of randomly oriented homogenized plies within a macroscopically homogenous multi-laminate system [43]. The arithmetic mean of $\mathbb{A}$ encountered in the training data used in this study is 17.4 while previous studies involving hcp single crystals encountered a mean anisotropic index of 2.2 [26].

A total of 860 simulations were sequentially added (1600 simulations total) to achieve convergence in the model building process. Convergence in the model building process is determined by changes in the model coefficients, $\boldsymbol{A}$, established at every step.

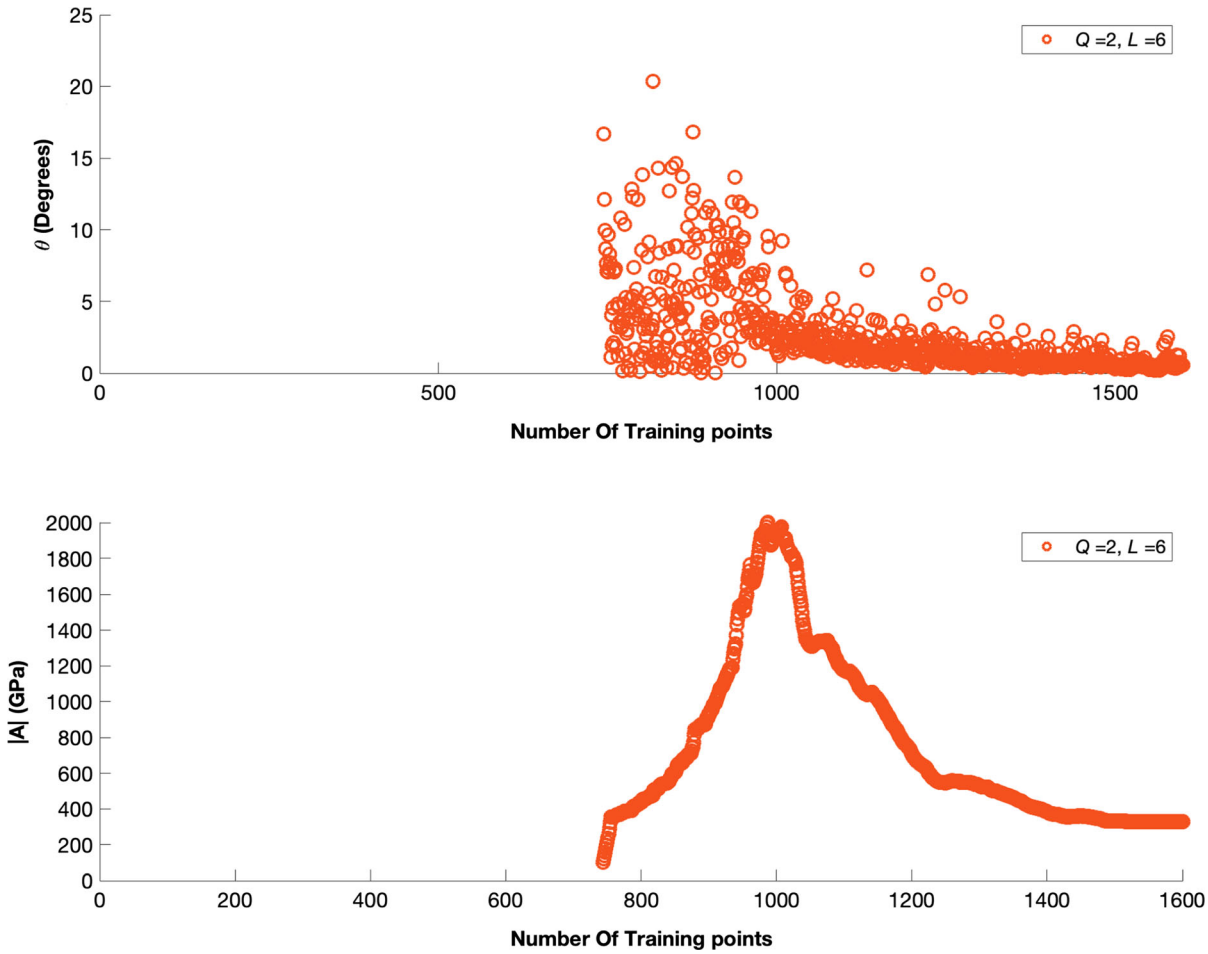

Fig. 1 Convergence metrics during the building of the reduced-order model developed in this work, corresponding to truncation levels Q = 2, L = 6. Top: The angular difference of the vector of model coefficients due to the addition of new simulations is shown to converge around 1600 simulations. Bottom: The magnitude of the vector of model coefficients shows a similar convergence

Changes in the model coefficients as simulations are added is shown in Fig. 1. It is seen that the model building process described in this paper produces a robust model.

An additional 600 simulations were added via the sequential design process for critical validation of the predictive performance of the reduced-order model. The accuracy of the predictions over the training and test sets is summarized in Fig. 2. The reduced-order-model produced in this work shows very good predictive capability, exhibiting a mean absolute prediction error of 0.75 GPa over the test set. We note, predictions with a relatively high error (greater than 3.5 GPa) consistently corresponded to high values of $\mathbb{A}$ ranging from 75 to 215.

3.2 Estimation of single ply stiffness from indentation measurements

We now shift focus to sampling the posterior distribution of ply elastic constants, $\boldsymbol{c} = \{C_{11}, C_{12}, C_{44}, C_{33}, C_{13}\}$, given a set of experimentally measured indentation moduli at different declination angles in individual plies of a multi-laminate sample. Following the establishment of the reduced-order model in the previous subsection, the likelihood function in Eq. (3) can readily be evaluated for the available experimental data (presented in Table 1). In accordance with the methodology described earlier, 50,000 samples are drawn from the posterior distribution shown in Eq. (4) using a Single

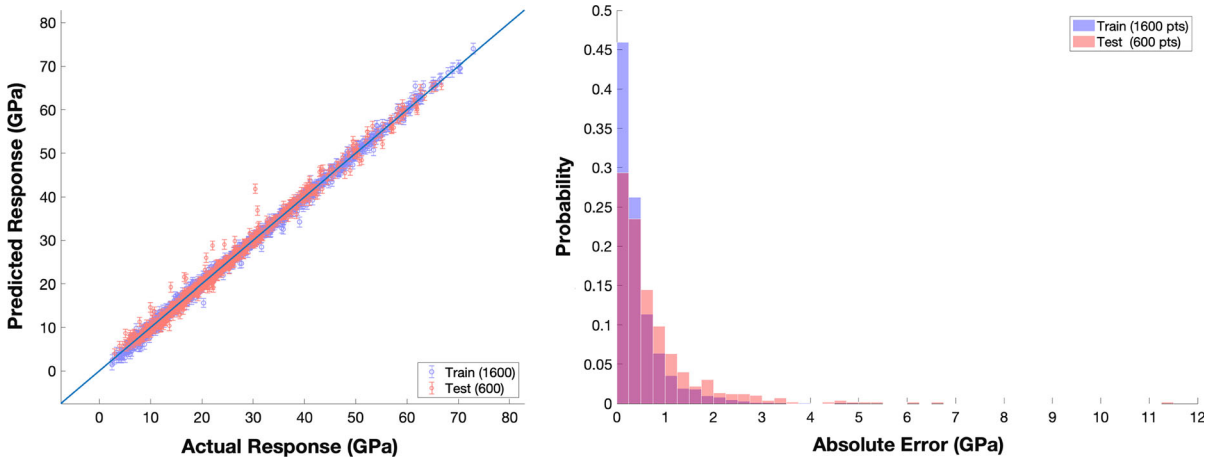

Fig. 2 The accuracy of the reduced-order model built in this work for the prediction of the FE simulated effective indentation modulus for input values of the single ply stiffness distributed over the ranges specified in Table 2 and ply orientations ranging between 0° and 90°. Left: Comparison of predicted and actual FE simulated effective indentation modulus for test and training data. Right: Corresponding histograms of the absolute error for test data and training data

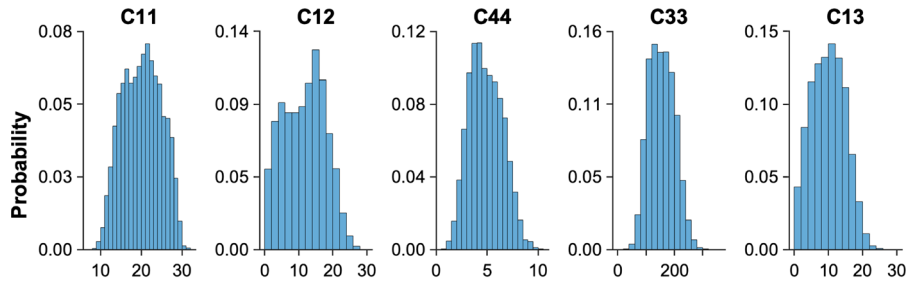

	C11	C12	C44	C33	C13
Mean (GPa)	20.1	11.7	4.9	155.4	9.9
STDEV	4.7	6.1	1.6	45.2	4.9

Fig. 3 Extracted posterior distributions of the single ply elastic stiffness parameters from the available experimentally measured indentation moduli presented in Table 1

Component Metropolis–Hastings algorithm [26]. The sampled posterior distributions of the effective elastic constants are shown in Fig. 3. The mean values were found to be $\boldsymbol{c} = \{20.1, 11.7, 4.9, 155.4, 9.9\}$GPa.

Literature regarding the extraction of the (homogenized) single ply elastic properties from multi-laminate samples is sparse. To provide a basis for comparison, the effective properties of a corresponding ply with a fiber volume fraction of 63% (reported in the experiments) estimated using Eqs. (7–11) [29] is shown in Table 3.

Interestingly, all of the estimates obtained using the simplified equations presented in Eqs. (7–11) lie close to or within a single standard deviation of the respective sampled means. The noticeably higher discrepancy for the value of C_{11} is consistent with observations in prior experimental work when comparing the experimental data in Table 1 to FE simulations using initial effective property estimates [29]. We emphasize that one of the main advantages of the proposed framework is that we obtain useful measures of the uncertainty related to the estimated single ply elastic stiffness parameters from the spherical indentation measurements. Note that the uncertainty is relatively higher for the estimates of the "off diagonal" stiffness constants, C_{12} and C_{13}. This is because the indentation modulus exhibits a relatively low sensitivity to changes in these parameters across

Table 3 Comparison of effective elastic constants extracted using MCMC to estimates [29] obtained using Eqs. (7–11). We note the sampled distributions provide a measure of uncertainty with respect to the extracted ply elastic stiffness constants

	C_{11} (GPa)	C_{12} (GPa)	C_{44} (GPa)	C_{33} (GPa)	C_{13} (GPa)
V_f: 63%	15.1	8.0	4.9	179.6	7.2
Sampled mean	20.1 ± 4.7	11.7 ± 6.1	4.9 ± 1.6	155.4 ± 45.2	9.9 ± 4.9

the ply-orientation space [44]. The relatively high uncertainty levels in Table 3 could be reduced if additional indentation measurements at additional ply orientations become available. Determination of where to perform additional experiments can be qualitatively determined by viewing the predictions of the reduced-order model over the ply orientation space. The variation in the predictions of the reduced-order model due to the MCMC process is shown in Fig. 4.

The predictions of the variation of the indentation moduli with the indentation declination angle, obtained from MCMC sampling, conform closely to the measured experimental indentation dataset verifying that the underlying variation in local indentation modulus observed within the single plies is effectively being communicated to the extracted distributions. However, significant variation in predictions occurs at lower declination angles, suggesting there would be value from additional experiments performed at lower declination angles. We note that the recently developed work in the sequential selection of indentation experiments based on highest information gain [45] may prove useful in leveraging the extracted distributions of effective elastic constants in order to quantitatively determine the precise orientation of single plies to focus upon that may best sharpen the C_{12} and C_{13} distributions.

3.3 Bulk multi-laminate property estimation

The effective elastic properties of a multi-laminate system can be tailored by manipulating the configuration of the constituent plies. Simple homogenization theories have often provided estimates for the effective properties of various configurations of a multi-

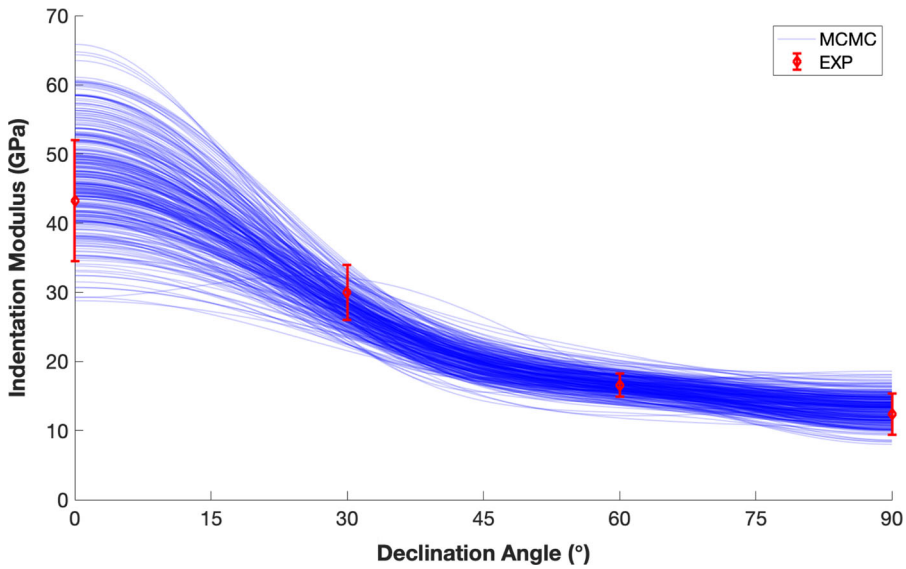

Fig. 4 The sampled MCMC posterior distribution for the prediction of indentation moduli as a function of the indentation declination angle. Highest uncertainty is seen at low declination angles, suggesting more information gathered at these angles will provide the best improvement in the extracted effective intrinsic properties

Table 4 Comparison of homogenized longitudinal Young's Modulus predicted using posterior distributions of single ply elastic stiffness constants to the longitudinal Young's Modulus measured experimentally for multiple multi-laminate configurations

Multi-laminate Ply configuration	Experimental longitudinal Young's modulus	Expected longitudinal Young's modulus	STDEV of expected longitudinal Young's modulus
$[0/+45/90/-45]_{2S}$	58.9	57.6	0.6
$[+60/0/-60]_{3S}$	59.5	57.9	0.6
$[+30/+60/90/-60/-30]_{2S}$	38.1	39.5	0.4

laminate system. Therefore, it is desirable to incorporate the distributions of effective elastic constants sampled in Sect. 3.2 into such homogenization schemes in order to examine how the uncertainty in the single ply properties are propagated to the effective properties at the next higher length scale. Specifically, the overall elastic properties of a multi-laminate system with m oriented plies can be estimated using an iso-strain model [6, 7] expressed as

$$\bar{\mathrm{C}}_{ijkl} = f(\boldsymbol{c}) = \sum_{t=1}^{m} \mathrm{C}_{pqrs} V^t Q^t_{ip} Q^t_{jq} Q^t_{kr} Q^t_{ls} \tag{13}$$

where C denotes the 4th rank elastic stiffness tensor composed from $\boldsymbol{c}$, V^t is the volume fraction of the tth ply and Q^t denotes the rotation matrix which transforms the material principle frame to the sample frame in accordance with the t-th ply orientation. We note, $\bar{\mathrm{C}}$ is the effective 4th rank stiffness tensor of the multi-laminate system. In practice, symmetric ply configurations are often chosen such that a multi-laminate system likely exhibits an orthotropic, or quasi-isotropic elastic response [5, 38, 46, 47]. Consequently, the effective Young's modulus in the longitudinal direction of such multi-laminate systems is commonly reported in experiments [38, 48]. Let $g(\bar{\mathrm{C}})$ be the function which computes the effective Young's modulus, denoted $\bar{E}$, in the longitudinal direction of an elastic orthotropic or quasi-isotropic multi-laminate system. We recall this relation is readily available in literature [5]. In order to take into account the distributions of effective elastic constants extracted in Sect. 3.2, the *expected* effective Young's modulus, can be computed as

$$\mathbb{E}\left(\bar{E}|\boldsymbol{E}^*_{exp}, \boldsymbol{\Phi}_{exp}, \boldsymbol{c}\right) = \int g(f(\boldsymbol{c})) p(\boldsymbol{c}|\boldsymbol{E}^*_{exp}, \boldsymbol{\Phi}_{exp}) d\boldsymbol{c} \tag{14}$$

where the expectation function, $\mathbb{E}$, is readily approximated using the Monte-Carlo estimate [49] by

$$\mathbb{E}\left(\bar{E}|\boldsymbol{E}^*_{exp}, \boldsymbol{\Phi}_{exp}, \boldsymbol{c}\right) \approx \frac{1}{N} \sum_{i=1}^{N} g(f(\boldsymbol{c}_i)) \tag{15}$$

where $\boldsymbol{c}_i$ enumerates the $N = 50,000$ samples of the Markov Chain. The expected effective Young's Moduli in the longitudinal direction computed for various configurations of the IM7/977-3 epoxy-carbon fiber multi-laminate system are compared to previously reported experimentally measured values [38] in Table 4.

The computed expected longitudinal stiffness using the distributions extracted in Sect. 3.2 are in very good agreement with experimentally measured values. Furthermore, the reported standard deviations correspond to 10 separate MCMC chains. The small deviations between the predictions of these chains indicate robustness of the MCMC sampling methodology. The above exercise demonstrates how the distributions of in-situ elastic ply properties may provide accurate predictions of the homogenized properties for arbitrary configurations of multi-laminate composite systems.

4 Conclusions

A new framework has been presented and demonstrated for the extraction of homogenized single ply anisotropic elastic constants from available spherical indentation measurements on single plies within a multi-laminate PMC sample. The available experimental measurements exhibited varying levels of variance attributed to a large variance in the local fiber volume fractions in the primary zones of indentation. The Bayesian framework extended from prior work was successfully employed to sample distributions of the ply anisotropic elastic constants which reflect the uncertainty (expressed as variance) in the underlying experimental measurements. This is accomplished through the establishment of a

likelihood function which requires a FE model of the spherical indentation experiment. In practice, a large number of evaluations of the likelihood function is necessary to discern the distributions of effective elastic constants. In order to expedite these computations, a high fidelity reduced-order model is established for the FE model of the indentation measurement. Following the determination of the distribution of effective elastic constants pertaining to single plies, high fidelity estimates of bulk elastic properties of multi-laminate samples with various ply configurations were obtained. This was accomplished using the extracted distributions of effective elastic constants coupled with existing composite lamina theory.

Acknowledgements The authors acknowledge support from ONR Grant N00014-18-1-2879.

Compliance with ethical standards

Conflict of interest The authors declare they have no conflict of interest.

References

1. Koronis G, Silva A, Fontul M (2013) Green composites: a review of adequate materials for automotive applications. Compos B 44(1):120–127. https://doi.org/10.1016/j.compositesb.2012.07.004
2. Soutis C (2005) Fibre reinforced composites in aircraft construction. Prog Aerosp Sci 41(2):143–151. https://doi.org/10.1016/j.paerosci.2005.02.004
3. Hollaway LC (2010) A review of the present and future utilisation of FRP composites in the civil infrastructure with reference to their important in-service properties. Constr Build Mater 24(12):2419–2445. https://doi.org/10.1016/j.conbuildmat.2010.04.062
4. Mouritza AP, Bannister MK, Falzonb PJ, Leongb KH (1999) Review of applications for advanced three-dimensional fibre textile composites. Compos A Appl Sci Manuf 30:1445–1461
5. Reddy JN, Miravete A (2018) Practical analysis of composite laminates. CRC Press, Boca Raton
6. Chamis CC (1989) Mechanics of composite-materials—past, present, and future. J Compos Technol Res 11(1):3–14
7. Kalidindi SR, Franco E (1997) Numerical evaluation of isostrain and weighted-average models for elastic moduli of three-dimensional composites. Compos Sci Technol 57(3):293–305
8. Pastore C, Gowayed Y (2008) 6—Structure and mechanics of 2D and 3D textile composites. In: Schwartz P (ed) Structure and mechanics of textile fibre assemblies. Woodhead Publishing, Cambridge, pp 141–189. https://doi.org/10.1533/9781845695231.141
9. Kregers AF, Melbardis YG (1978) Determination of the deformability of three-dimensionally reinforced composites by the stiffness averaging method. Polym Mech 14(1):1–5. https://doi.org/10.1007/BF00859550
10. Ishikawa T, Chou TW (1982) Stiffness and strength behaviour of woven fabric composites. J Mater Sci 17(11):3211–3220. https://doi.org/10.1007/BF01203485
11. Reddy JN (2003) Mechanics of laminated composite plates and shells: theory and analysis. CRC Press, Boca Raton
12. Barbero E, Reddy J (1990) Nonlinear analysis of composite laminates using a generalized laminated plate theory. AIAA J 28(11):1987–1994
13. Flaggs DK, Kural MH (1982) Experimental determination of the in situ transverse lamina strength in graphite/epoxy laminates. J Compos Mater 16:103–116
14. Huang ZM (2001) Simulation of the mechanical properties of fibrous composites by the bridging micromechanics model. Compos Part A Appl Sci 32(2):143–172. https://doi.org/10.1016/S1359-835x(00)00142-1
15. Kalidindi SR, Abusafieh A (1996) Longitudinal and transverse moduli and strengths of low angle 3-D braided composites. J Compos Mater 30(8):885–905
16. Engelstad S, Reddy J (1993) Probabilistic nonlinear finite element analysis of composite structures. AIAA J 31(2):362–369
17. Hardiman M, Vaughan TJ, McCarthy CT (2017) A review of key developments and pertinent issues in nanoindentation testing of fibre reinforced plastic microstructures. Compos Struct 180:782–798. https://doi.org/10.1016/j.compstruct.2017.08.004
18. Hodzic A, Kalyanasundaram S, Kim JK, Lowe AE, Stachurski ZH (2001) Application of nano-indentation, nano-scratch and single fibre tests in investigation of interphases in composite materials. Micron 32(8):765–775. https://doi.org/10.1016/S0968-4328(00)00084-6
19. Vlassak JJ, Nix WD (1994) Measuring the elastic properties of anisotropic materials by means of indentation experiments. J Mech Phys Solids 42(8):1223–1245. https://doi.org/10.1016/0022-5096(94)90033-7
20. Unnikrishnan GU, Unnikrishnan VU, Reddy JN (2006) Constitutive material modeling of cell: a micromechanics approach. J Biomech Eng 129(3):315–323. https://doi.org/10.1115/1.2720908
21. Pathak S, Stojakovic D, Kalidindi SR (2009) Measurement of the local mechanical properties in polycrystalline samples using spherical nanoindentation and orientation imaging microscopy. Acta Mater 57(10):3020–3028. https://doi.org/10.1016/j.actamat.2009.03.008
22. Weaver JS, Priddy MW, McDowell DL, Kalidindi SR (2016) On capturing the grain-scale elastic and plastic anisotropy of alpha-Ti with spherical nanoindentation and electron back-scattered diffraction. Acta Mater 117:23–34
23. Khosravani A, Morsdorf L, Tasan CC, Kalidindi SR (2018) Multiresolution mechanical characterization of hierarchical materials: spherical nanoindentation on martensitic Fe–Ni–C steels. Acta Mater 153:257–269. https://doi.org/10.1016/j.actamat.2018.04.063
24. Pathak S, Kalidindi SR, Mara NA (2016) Investigations of orientation and length scale effects on micromechanical responses in polycrystalline zirconium using spherical

nanoindentation. Scr Mater 113:241–245. https://doi.org/10.1016/j.scriptamat.2015.10.035
25. Pathak S, Kalidindi SR (2015) Spherical nanoindentation stress–strain curves. Mater Sci Eng R Rep 91:1–36
26. Castillo AR, Kalidindi SR (2019) A Bayesian framework for the estimation of the single crystal elastic parameters from spherical indentation stress–strain measurements. Front Mater 6:136
27. Patel DK, Al-Harbi HF, Kalidindi SR (2014) Extracting single-crystal elastic constants from polycrystalline samples using spherical nanoindentation and orientation measurements. Acta Mater 79:108–116. https://doi.org/10.1016/j.actamat.2014.07.021
28. Patel D, Kalidindi S (2017) Estimating the slip resistance from spherical nanoindentation and orientation measurements in polycrystalline samples of cubic metals. Int J Plast 92:19
29. Rossi A, Castillo A, Przybyla C, Kalidindi SR (2019) Study of local mechanical responses in an epoxy-carbon fiber laminate composite using spherical indentation stress-strain. integrating materials and manufacturing innovation (accepted)
30. Hertz H (1896) Miscellaneous papers. MacMillan and Co., Ltd., New York, p 146
31. Haario H, Saksman E, Tamminen J (2005) Componentwise adaptation for high dimensional MCMC. Comput Stat 20(2):265–273. https://doi.org/10.1007/BF02789703
32. Gelman A, Carlin J, Stern H, Dunson D, Vehtari A, Rubin D (2014) Bayesian data analysis, 3rd edn. Texts in statistical science. Chapman and Hall/CRC, Boca Raton
33. Roberts GO, Gelman A, Gilks WR (1997) Weak convergence and optimal scaling of random walk metropolis algorithms. Ann Appl Probab 7(1):110–120. https://doi.org/10.1214/aoap/1034625254
34. MacKay DJC (1992) Bayesian interpolation. Neural Comput 4(3):415–447. https://doi.org/10.1162/neco.1992.4.3.415
35. Bunge HJ (1993) Texture analysis in materials science. Mathematical methods (trans: Morris PR). Cuvillier Verlag, Göttingen
36. Kalidindi SR, Pathak S (2008) Determination of the effective zero-point and the extraction of spherical nanoindentation stress-strain curves. Acta Mater 56(14):3523–3532. https://doi.org/10.1016/j.actamat.2008.03.036
37. Barlat F, Maeda Y, Chung K, Yanagawa M, Brem JC, Hayashida Y, Lege DJ, Matsui K, Murtha SJ, Hattori S, Becker RC, Makosey S (1997) Yield function development for aluminum alloy sheets. J Mech Phys Solids 45(11):1727–1763. https://doi.org/10.1016/S0022-5096(97)00034-3
38. Clay SB, Knoth PM (2016) Experimental results of quasi-static testing for calibration and validation of composite progressive damage analysis methods. J Compos Mater 51(10):1333–1353. https://doi.org/10.1177/0021998316658539
39. Kaddour AS, Hinton MJ (2012) Input data for test cases used in benchmarking triaxial failure theories of composites. J Compos Mater 46(19–20):2295–2312. https://doi.org/10.1177/0021998312449886
40. Joseph VR, Gul E, Ba S (2015) Maximum projection designs for computer experiments. Biometrika 102(2):371–380
41. ABAQUS (2014) 6.14 Dassault Systémes Simulia Corp. Providence, RI
42. Christopher MB (2006) Pattern recognition and machine learning. Springer, New York
43. Ranganathan SI, Ostoja-Starzewski M (2008) Universal elastic anisotropy index. Phys Rev Lett 101(5):055504. https://doi.org/10.1103/PhysRevLett.101.055504
44. Sobol′ IM (2001) Global sensitivity indices for nonlinear mathematical models and their Monte Carlo estimates. Math Comput Simul 55(1):271–280. https://doi.org/10.1016/S0378-4754(00)00270-6
45. Castillo AR, Joseph VR, Kalidindi SR (2019) Bayesian sequential design of experiments for extraction of single-crystal material properties from spherical indentation measurements on polycrystalline samples. JOM 71:2671–2679
46. Staab GH (1999) 6—Laminate analysis. In: Staab GH (ed) Laminar composites. Butterworth-Heinemann, Woburn, pp 191–282. https://doi.org/10.1016/B978-075067124-8/50006-0
47. Khdeir AA, Reddy JN (1989) Exact solutions for the transient response of symmetric cross-ply laminates using a higher-order plate theory. Compos Sci Technol 34(3):205–224. https://doi.org/10.1016/0266-3538(89)90029-8
48. ASTM D (2008) Standard test method for tensile properties of polymer matrix composite materials
49. Caflisch RE (1998) Monte Carlo and quasi-Monte Carlo methods. Acta Numer 7:1–49. https://doi.org/10.1017/S0962492900002804